

## High-Resolution Scanning Tunneling Spectroscopy of Magnetic Impurity Induced Bound States in the Superconducting Gap of Pb Thin Films

Shuai-Hua Ji,<sup>1,2</sup> Tong Zhang,<sup>1,2</sup> Ying-Shuang Fu,<sup>1,2</sup> Xi Chen,<sup>1,\*</sup> Xu-Cun Ma,<sup>2</sup> Jia Li,<sup>1</sup> Wen-Hui Duan,<sup>1</sup>  
Jin-Feng Jia,<sup>1</sup> and Qi-Kun Xue<sup>1,2,†</sup>

<sup>1</sup>*Department of Physics, Tsinghua University, Beijing 100084, China*

<sup>2</sup>*Institute of Physics, Chinese Academy of Sciences, Beijing 100080, China*

(Received 17 December 2007; published 5 June 2008)

Tunneling spectra for individual atoms and dimers of Mn and Cr adsorbed on superconducting Pb thin films were measured by a low temperature scanning tunneling microscope. Multiple-resonance structures within the superconducting gap on the adsorbates were resolved and interpreted as the magnetic impurity-induced bound states associated with different scattering channels. The experiment demonstrates a spectroscopic approach to characterizing the spin states of magnetic structures and exploring the competition between superconductivity and magnetism at the nanometer scale.

DOI: [10.1103/PhysRevLett.100.226801](https://doi.org/10.1103/PhysRevLett.100.226801)

PACS numbers: 74.78.Db, 68.37.Ef, 74.50.+r, 75.75.+a

A magnetic impurity in a superconductor breaks the time-reversal symmetry and induces low energy bound states in the superconducting gap [1–3]. Probing the response of superconductors to magnetic impurities has been one of the important methods for revealing the nature of the superconducting pairing [4]. On the other hand, the intragap states offer a sensitive mechanism to detect the spin states of the magnetic impurities. The magnetic impurity-induced bound states in a conventional superconductor were previously observed in a scanning tunneling microscopy (STM) study by Yazdani *et al.* [5]. The tunneling spectra in their experiments reveal an enhancement of the density of the excitations within the superconductor's gap near the magnetic adsorbates. However, it remains challenging to make use of these intragap resonances in analyzing the spin states of adsorbates, in part because of the insufficient energy resolution. For example, the splitting of the intragap states induced by magnetic coupling between impurities is typically 1 order of magnitude smaller than the superconducting gap and thereby cannot be easily resolved by an STM. Here we report a scanning tunneling spectroscopic (STS) study of the magnetic atom-induced bound states in a superconducting Pb thin film, which can explicitly resolve the multiple scattering channels and introduces a novel approach for extracting the spin information of impurities at the single atomic level [6–10].

Our experiments were conducted with a Unisoku UHV <sup>3</sup>He STM system [11]. Pb (with purity of 99.999%) was deposited on the clean Si(111) – 7 × 7 surface at room temperature and further annealed for 30 min to form atomically flat films [12] with a lateral extension of 200 nm, which is much larger than the superconducting coherence length (~ 30 nm) [13]. In the present experiment, a film with a thickness of 20 monolayers (ML) was chosen as the substrate whose averaged superconducting gap  $\Delta_{\text{sample}}$  was 1.30 meV determined by STS measurement [14].

Several measures have been taken to achieve enhanced tunneling junction stability and high spectroscopic resolu-

tion, which include: (a) elaborate grounding and shielding scheme to minimize the electrical noises; (b) 0.4 K base temperature by means of a single-shot <sup>3</sup>He cryostat to reduce the thermal broadening and drift; and (c) a superconductive Nb STM tip to improve the energy resolution by utilizing the sharp change in the density of states at the superconducting gap edges. As a result, the energy resolution of STS reaches ~0.1 meV at 0.4 K. Nearly ideal differential conductance was obtained for the superconductor-superconductor (*S-S*) tunneling junction formed by the Nb tip and the Pb film [illustrated in Fig. 1(a)] via lock-in detection of the first harmonic in the tunneling current. Figure 1(b) clearly reveals the characteristic *S-S* tunneling peaks at  $\pm(\Delta_{\text{tip}} + \Delta_{\text{sample}})$ . The superconducting gap  $\Delta_{\text{tip}}$  of the tip was found to be 1.52 meV by fitting the conductance using the BCS density of states for Pb and Nb with  $\Delta_{\text{sample}} = 1.30$  meV and  $T = 0.4$  K [solid curve in Fig. 1(b)]. Depending on the tips,  $\Delta_{\text{tip}}$  may vary between 1.44 and 1.52 meV [15], and was determined individually by measuring the tunneling conductance of the *S-S* junction on bare Pb film.

The transition metal (Mn and Cr) atoms were deposited on the Pb film (111) surface at about 30 K. At a coverage of 0.0006 ML, the well-isolated metal atoms of both Mn and Cr are imaged as round protrusions [Fig. 1(c) for Mn, and Fig. 1(e) for Cr]. The STS from –2.8 meV to +2.8 meV (between the two *S-S* tunneling peaks) on the adatoms exhibit the well-defined resonance structures [Figs. 1(d) and 1(f)] due to the formation of the bound states. Four peaks for Mn and six for Cr are explicitly resolved, respectively. The spectra, as the “fingerprints” of the spin states, involve two groups of resonances, i.e., the electronlike states seen at the positive bias and the holelike states seen at the negative bias [5,16–18]. Whereas the positions of the electronlike and the holelike resonances are symmetric with respect to the zero bias, their amplitudes are asymmetric as a result of the broken symmetry under the particle-hole transformation. Evidently, these peaks origi-

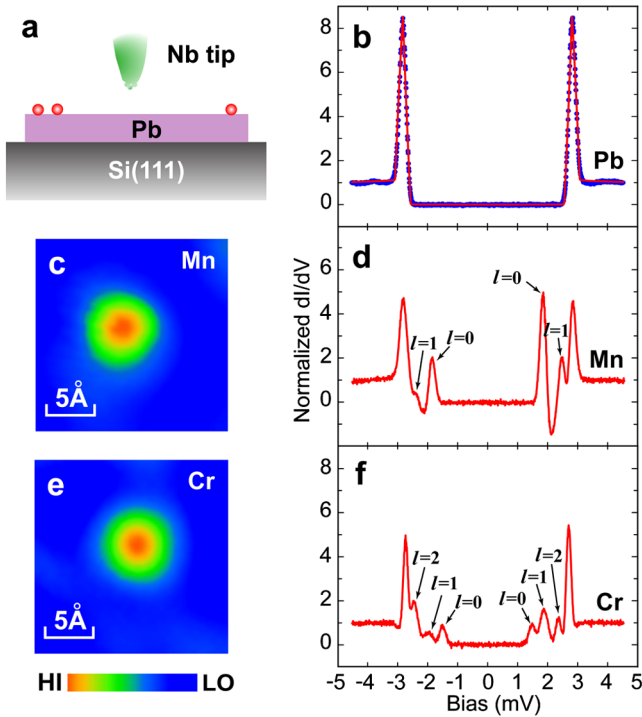


FIG. 1 (color online). Single magnetic atom-induced bound states in the superconducting gap of Pb thin films. (a) Schematic and (b) differential conductance of the  $S$ - $S$  tunneling junction. The tunneling junction was set at  $V_{\text{bias}} = 10$  mV,  $I = 0.4$  nA. The bias modulation was 0.05 mV (rms) at 1.991 kHz. (c)–(f) Topographic images and normalized  $dI/dV$  spectra of single Mn and Cr atoms at 0.4 K. For a Mn atom (c), the four peaks at energies of  $-2.35$  meV,  $-1.84$  meV,  $+1.86$  meV, and  $+2.47$  meV correspond to the first two angular momentum channels, respectively. For a Cr atom (e), six peaks (f) were detected at energies of  $-2.44$  meV,  $-1.92$  meV,  $-1.49$  meV,  $+1.49$  meV,  $+1.89$  meV, and  $+2.38$  meV, respectively. The plus and minus signs correspond to the electronlike and holelike excitations. Suppressing of the coherence peaks of superconductor by the magnetic atoms is noted.

nate from the interaction between the magnetic atoms and the superconducting host since they disappeared completely when a 3 T magnetic field was applied perpendicularly to quench the superconductivity of the Pb film.

The multiple-peak structure has its origin in the different angular momentum channels ( $l = 0, 1, 2$ , etc.) in scattering, and is directly related to the magnetic moment of the impurity. In the limit of classical spin, the binding energy [3] for a localized bound state is

$$E_l = \Delta_0 \cos(\delta_l^+ - \delta_l^-), \quad (1)$$

where  $\Delta_0$  is the superconducting gap and  $\delta_l^\pm$  are the phase shifts for the scattering of spin up (+) and spin down (−) quasiparticles off a magnetic impurity in the  $l^{\text{th}}$ -angular momentum channel. The partial waves beyond  $l = 0$  have been essential to obtain an accurate description of the magnetic impurities in a superconducting host [19,20].

Further comparison with theory would require a thorough electronic structure calculation.

The order-parameter relaxation also provides a local attractive potential for quasiparticles and produces bound states in the superconducting gap at the energy

$$\Omega_0 = \Delta_0 \sqrt{1 - \alpha^2}, \quad (2)$$

where  $\alpha$  is a parameter related to the suppression of the gap function  $\delta\Delta$  and the Coulomb potential of the impurity [18]. However, weak gap function suppression ( $\delta\Delta \ll \Delta_0$ ) is indicated by comparing STS measured on the bare Pb surface and those on the isolated magnetic impurities in Fig. 1, refuting the possibility of attributing the observed resonances to order-parameter relaxation. The suppression of gap function at the impurity sites is negligible in the weak coupling limit where the ground state of the superconductor is still a paired state of the time-reversed single-particle states [18]. Nevertheless, the lower coherence peaks in the spectra on a magnetic atom indicate that the lifetime of the quasiparticles is distinctly decreased by the magnetic impurities.

The spectra in Fig. 1 are the convolution of the density of states of the superconducting tip with that of the substrate. The gap function of the Nb tip can be determined by the BCS density of states of the Pb film together with the STS on the bare Pb surface with the same tip. Numerical deconvolution was performed to find the energies of the bound states induced by single Mn and Cr atoms, as well as the Mn dimer discussed later. The results are summarized in Table I.

The significance of the experiments is best demonstrated by characterizing the local electronic properties of Mn and Cr dimers via the intragap bound states. Dimers of both Mn and Cr could be easily obtained by increasing the coverage of the atoms deposited. Because of the higher concentration of magnetic impurities, the discrete bound states develop into impurity bands [20–22] inside the superconducting gap. The formation of the impurity bands is evident in the STS taken on the bare Pb surface far away from the adatoms, as indicated by the arrows in Figs. 2(c) and 4(c).

Figures 2(a) and 2(b) show two different Mn dimer configurations. The interatomic distances and the height difference between the neighboring Mn atoms in the topographic images imply nonequivalent adsorption sites for the two atoms in a dimer. It has been predicted theoretically [23–25] that the atomlike bound states of the two impurities in a dimer will hybridize and split into bonding and antibonding states if the magnetic moments of the impurities are parallel. The effect of interaction between the two Mn atoms in a dimer is clearly revealed by the  $dI/dV$  spectra [Fig. 2(c)] and the spatial mappings (Fig. 3) of the resonances. Both  $l = 0$  and  $l = 1$  peaks split in Mn dimer II, indicating a ferromagnetic coupling between the two Mn atoms at 4.2 Å. In the case of a dimer at larger

TABLE I. Binding energies for the intragap states. The energies are the peak positions in the spectral density of the superconducting Pb with respect to the chemical potential. Plus and minus signs outside the parenthesis correspond to the electronlike and the holelike states, respectively.

Energy (meV)	Mn atom	Cr atom	Mn dimer II
$E(l=0)$	$\pm(0.38 \pm 0.02)$	$\pm(0.17 \pm 0.04)$	$\pm(0.06 \pm 0.03)$
$E(l=1)$	$\pm(1.02 \pm 0.03)$	$\pm(0.53 \pm 0.03)$	$\pm(0.39 \pm 0.02)$
$E(l=2)$	...	$\pm(1.03 \pm 0.03)$	$\pm(0.88 \pm 0.03)$
$E(l=3)$	...	...	$\pm(1.22 \pm 0.02)$

distance (Mn dimer I), only the  $l=0$  peak splits, which may result from different alignment other than purely ferromagnetic.

Although both Mn dimer I and II show explicit interference feature in the  $dI/dV$  mappings, their patterns are qualitatively different (Fig. 3). More specifically, while the local density of electronic states (LDOS) of the Mn dimer at 6.1 Å appears to be the even and odd combinations of the unhybridized bound states [Figs. 3(d)–3(g)], the split states for each scattering channel of the 4.2 Å dimer consist of two roughly complementary components in the spatial distribution [Figs. 3(h)–3(k) for electronlike and 3(l)–3(o) for holelike states], i.e., the LDOS of one state is high in the region where that of the other is low, and vice versa. The intriguing mapping for Mn dimer II may arise from the stronger coupling between Mn atoms at shorter interatomic distance, where the picture based on simple hybridization is no longer applicable.

The situation for Cr is strikingly different (Fig. 4). While the spectrum of a dimer at 6.6 Å (Cr dimer I) is similar to

that of a single Cr atom, no intragap resonance has been observed for a dimer at 3.0 Å (Cr dimer II); the spectra of dimer II and the background (the Pb surface) are identical. The disappearance of the bound states is attributed to the antiferromagnetic coupling between the two Cr atoms in a dimer [26,27], which behaves like a nonmagnetic impurity with the total spin of zero. The bound state induced by a nonmagnetic impurity on a conventional  $s$ -wave superconductor such as Pb lies essentially at the gap edge with much smaller magnitude [4] and cannot be resolved by STS.

In conclusion, we have probed the intragap bound states induced by magnetic impurities in a superconductor using STS with high energy resolution. The study provides a novel approach to characterizing the development of impurity bands from individual bound states, and can conceivably lead to deeper understanding of the interplay between magnetism and superconductivity at the atomic

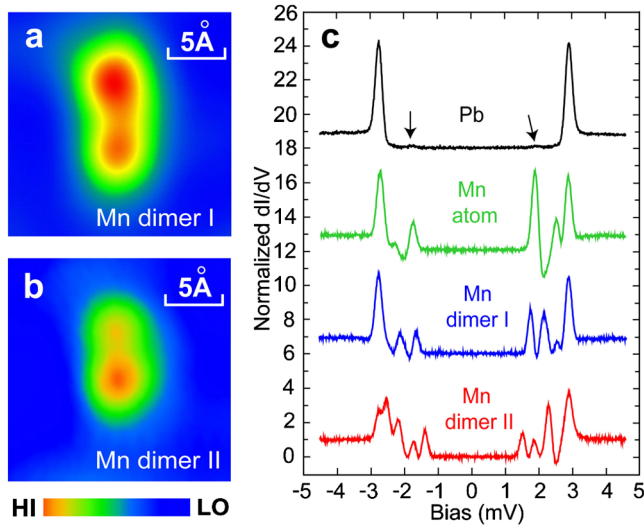


FIG. 2 (color online). (a) The topographic image of Mn dimer I with 6.1 Å interatomic distance. (b) The topographic image of Mn dimer II with 4.2 Å interatomic distance. (c) Typical  $dI/dV$  spectra taken on Pb (away from adsorbates), an isolated Mn atom, Mn dimer I, and Mn dimer II. The curves in (c) are offset vertically for clarity. All STS were acquired at a set point of  $V = 10$  mV and  $I = 0.2$  nA at 0.4 K.

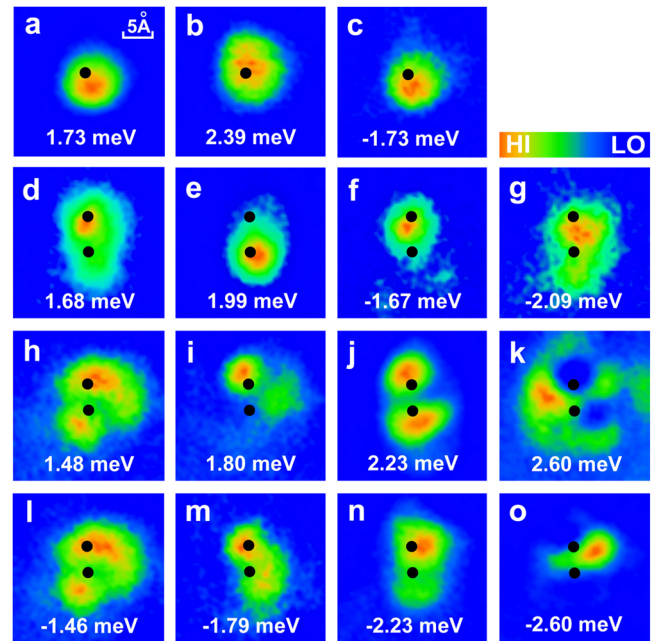


FIG. 3 (color online). (a)–(c) The  $dI/dV$  mappings for an isolated Mn atom at various energies. The holelike  $l=1$  state (not shown) is not strong enough for clear  $dI/dV$  imaging. (d)–(g)  $dI/dV$  mappings of Mn dimer I. (h)–(o)  $dI/dV$  mappings of Mn dimer II. The black dots indicate the centers of the atoms. Imaging conditions:  $V = 10$  mV and  $I = 0.15$  nA.

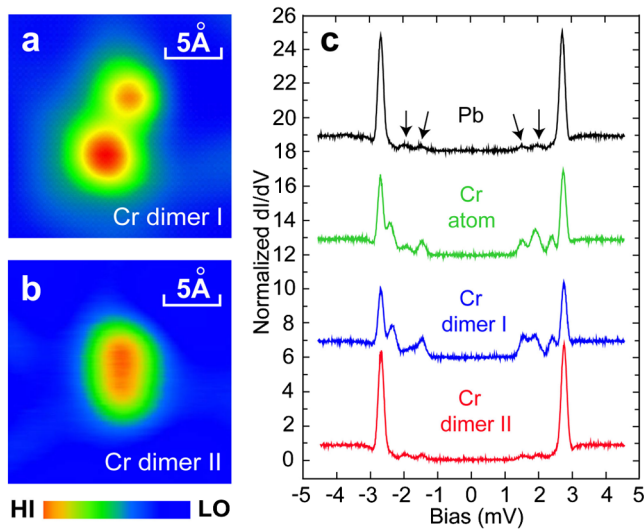


FIG. 4 (color online). (a) The topographic image of Cr dimer I with 6.6 Å interatomic distance. (b) The topographic image of Cr dimer II with 3.0 Å interatomic distance. (c) Typical  $dI/dV$  spectra taken on Pb (away from adsorbates), an isolated Cr atom, Cr dimer I and Cr dimer II. The curves in (c) are offset vertically for clarity. All STS were acquired at a set point of  $V = 10$  mV and  $I = 0.2$  nA at 0.4 K.

scale. The present method can be applied to various magnetic adatoms on a superconductor, which is not necessarily to be Pb. We expect that the experiments will also motivate further theoretical studies and stimulate more measurements, such as on the quantum phase transitions associated with multiple impurities [25].

We thank X. H. Qiu and C. J. Wu for discussions. This work was supported by National Natural Science Foundation and Ministry of Science and Technology of China. The STM topographic images were processed using WSxM [28].

\*xc@mail.tsinghua.edu.cn

†qkxue@mail.tsinghua.edu.cn

[1] L. Yu, *Acta Phys. Sin.* **21**, 75 (1965).

[2] H. Shiba, *Prog. Theor. Phys.* **40**, 435 (1968).

- [3] A. I. Rusinov, *Zh. Eksp. Teor. Fiz.* **56**, 2047 (1969) [*Sov. Phys. JETP* **29**, 1101 (1969)].
- [4] A. V. Balatsky, I. Vekhter, and J.-X. Zhu, *Rev. Mod. Phys.* **78**, 373 (2006).
- [5] A. Yazdani *et al.*, *Science* **275**, 1767 (1997).
- [6] A. J. Heinrich *et al.*, *Science* **306**, 466 (2004).
- [7] C. F. Hirjibehedin, C. P. Lutz, and A. J. Heinrich, *Science* **312**, 1021 (2006).
- [8] D. Kitchen *et al.*, *Nature (London)* **442**, 436 (2006).
- [9] C. F. Hirjibehedin *et al.*, *Science* **317**, 1199 (2007).
- [10] Y. Yayan, V. W. Brar, L. Senapati, S. C. Erwin, and M. F. Crommie, *Phys. Rev. Lett.* **99**, 067202 (2007).
- [11] Y.-S. Fu *et al.*, *Phys. Rev. Lett.* **99**, 256601 (2007).
- [12] Y. Guo *et al.*, *Science* **306**, 1915 (2004).
- [13] M. M. Özer, J. R. Thompson, H. H. Weitering, *Nature Phys.* **2**, 173 (2006).
- [14] In fitting the data with the BCS density of states, the anisotropy of the superconducting gap for Pb has been considered, see A. J. Bennett, *Phys. Rev.* **140**, A1902 (1965); G. I. Rochlin, *Phys. Rev.* **153**, 513 (1967).
- [15] S. H. Pan, E. W. Hudson, and J. C. Davis, *Appl. Phys. Lett.* **73**, 2992 (1998).
- [16] M. E. Flatté and J. M. Byers, *Phys. Rev. Lett.* **78**, 3761 (1997).
- [17] M. E. Flatté and J. M. Byers, *Phys. Rev. B* **56**, 11 213 (1997).
- [18] M. I. Salkola, A. V. Balatsky, and J. R. Schrieffer, *Phys. Rev. B* **55**, 12648 (1997).
- [19] A. B. Kunz and D. M. Ginsberg, *Phys. Rev. B* **22**, 3165 (1980).
- [20] J. K. Tsang and D. M. Ginsberg, *Phys. Rev. B* **22**, 4280 (1980).
- [21] L. Dumoulin, E. Guyon, and P. Nedellec, *Phys. Rev. B* **16**, 1086 (1977).
- [22] W. Bauriedl, P. Ziemann, and W. Buckel, *Phys. Rev. Lett.* **47**, 1163 (1981).
- [23] M. E. Flatté and D. E. Reynolds, *Phys. Rev. B* **61**, 14810 (2000).
- [24] D. K. Morr and N. A. Stavropoulos, *Phys. Rev. B* **67**, 020502(R) (2003).
- [25] D. K. Morr and J. S. Yoon, *Phys. Rev. B* **73**, 224511 (2006).
- [26] H. Cheng and L. S. Wang, *Phys. Rev. Lett.* **77**, 51 (1996).
- [27] T. Jammela, V. Madhavan, and M. F. Crommie, *Phys. Rev. Lett.* **87**, 256804 (2001).
- [28] www.nanotec.es.